## SCIENTIFIC AND TECHNICAL SECTION

## FINITE ELEMENT CALCULATION OF CLINCHING
## WITH RIGID DIE OF THREE STEEL SHEETS

**L. Kaščák,[a,1] E. Spišák,[a,2] R. Kubík,[a,3]**                    UDC 539.4
**and J. Mucha[b,4]**

*The clinching joining of three steel sheets (DC06, DX53D, and H220PD type) was studied by utilization of the finite element method. Clinched joints were also prepared experimentally by joining the above-mentioned steels with the thickness of 0.8 mm (DC06 and DX53D) and 1.0 mm (H220PD). The experimental tool works as single stroke tool, while prepared joints have circular axisymmetric shape, and the rigid die has no flexible segments. Finite element calculations were carried out in ANSYS software under simplified-axisymmetric conditions. Metallographic sections were also prepared from experimentally developed joints to make possible to directly compare the results of simulated and experimental approach. The results of computational approach are discussed and compared to the experimental ones.*

*Keywords:* finite element method (FEM), ANSYS, clinching, three sheets, steel, mechanical joining.

**Introduction.** Fast mechanical joining processes such as self-piercing riveting (SPR) and mechanical clinching (CL) represent viable solutions to meet the criteria such as employment of the new high-performance materials, improving the energy efficiency of products. Falling into the category of mechanical joining methods, they require no special preparation of surfaces. Mechanical clinching offers the additional advantage of not requiring an external component such as rivet, bolt, adhesive layer, etc. [1]. Mechanical joining clinching process is an effective joining method which includes the plastic deformation of the materials to be joined. Sheets ale deformed locally to generate an interlock between them. Mechanical clinching has been utilized to join coated, dissimilar, or hard to weld materials, such as aluminum alloy sheets [2]. It is also an environmentally friendly joining process due to low energy consumption, low-noise output, the absence of toxic emissions and heating, as compared to the resistance spot welding [3]. The plastic deformation of sheets is induced by the action of punch and die. Thus, the main limiting factor regarding joinability of a specific material is its formability. Because of distinctive advantages of the mechanical clinching with respect to equivalent joining processes, its suitability has been investigated over a large variety of materials, such as steel alloys, including aluminum, magnesium, titanium, as well as nonmetal materials, including polymers and wood. In the recent years, different modifications have been proposed to the original process to adapt the process to the specific needs, e.g., for joining of new and progressive materials with poor formability [4].

The mechanical joint forming process is shown in Fig. 1 and consists of totally four steps: start, drawing, compression, and interlocking. In the start phase, sheet materials are arranged over die cavity and clamped by sheet holder to prevent them from displacing. In the next step, two or more materials in the form of sheets are drawn into the die cavity by the downward motion of the punch. When the bottom sheet material reaches the surface of the die

[a]Technical University of Košice, Košice, Slovakia ([1]lubos.kascak@tuke.sk; [2]emil.spisak@tuke.sk; [3]rene.kubik@tuke.sk). [b]Rzeszów University of Technology, Rzeszów, Poland ([4]j_mucha@prz.edu.pl). Translated from Problemy Prochnosti, No. 4, pp. 6 – 18, July – August, 2017. Original article submitted September 1, 2017.
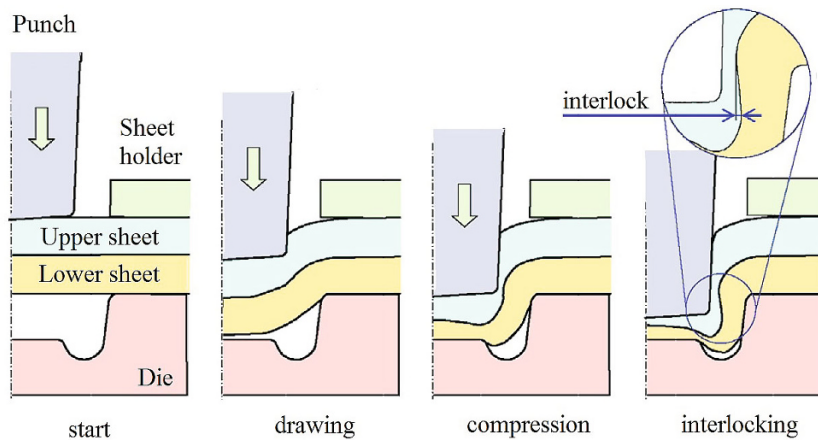
Fig. 1. The joint forming process in mechanical clinching with a rigid die [5].

cavity, the thickness of both sheets is being reduced by further downward motion of the punch. This phase is also known as the compression phase. An interlock is formed between the upper and lower sheet when material flows into the ring groove of the die cavity. The joint forming process ends when the specific level of forming force or displacement of the punch is reached.

**1. The Application of Finite Element Analysis (FEA) in Mechanical Clinching.** Large amount of scientific work has been done and published when it comes to simulation of the mechanical clinching process in general. When speaking in general terms, finite element analyses related to the mechanical clinching joining could be classified as follows:

(i) determination of the optimal shape and dimensions of the punch and die for clinching;

(ii) modification of the shape (e.g., $X$ parameter) of the joint in relation to its load-bearing capacity;

(iii) evaluation of the joint's properties (e.g., shear–tensile testing);

(iv) evaluation of the load of tools during mechanical joining;

(v) evaluation of the influence of process conditions (e.g., friction coefficient);

(vi) evaluation of the joinability of specific materials or combinations of materials (e.g., polymers);

(vii) testing of new variations of clinching joining (e.g., "hybrid resistance spot clinching");

(viii) prediction of the damage of materials during the joining process [e.g., cohesive zone model (CZM)].

FEA can be utilized to determine the individual geometry changes to the punch and die, which directly influence the interlocking and neck thickness of sheets. Various punch and die geometries can be designed and virtually tested by the FEA. The levels of interlocking between both sheets for individual geometries can be measured, and the optimal tool shape could be determined. Prior to that, resulting joints must be virtually loaded by force to determine their load-bearing capacity when having a specific level of interlocking [6]. Figure 2 shows the dependency between die depths and measured resulting values of neck thickness and undercut (interlocking).

FEA is also utilized when determining the optimal joining process parameters in relation to the geometry of the resulting clinched joint. The most critical parameters of the joint are interlocking and the bottom thickness of a clinched joint. The resulting bottom thickness of a joint depends on the depth of die, the level of joint forming force, or the stroke of a punch. It was determined by the FEA that increasing the die depth leads to the reduction of neck thickness and the increased undercut (or interlocking) in the resulting clinched joint (Fig. 2a). The effects of tool shape and process parameters are very similar  when joint's properties are evaluated. FEA was also utilized to investigate the influence of the bottom thickness of a joint on the joinability of advanced high-strength steels. The force required to form a clinched joint was gradually increased, which directly changed the bottom thickness of a mechanical joint and the level of interlocking between both steel sheets. Subsequently, the joints with different parameters were subjected to tensile and tensile–shear loadings. It was concluded that the greater the forming force level, the lower the bottom thickness value and the higher shear strength value of a joint. Tensile–shear tested clinched joint tends to fail by the neck fracture mechanism, which is related to the neck thickness of a mechanical
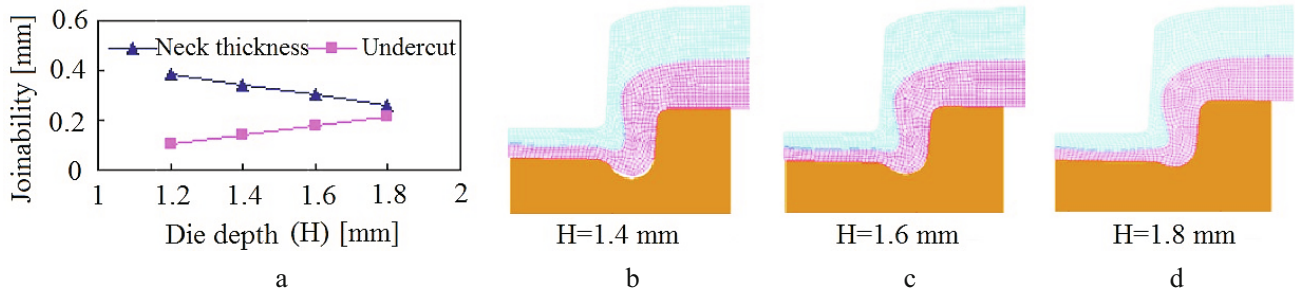
489

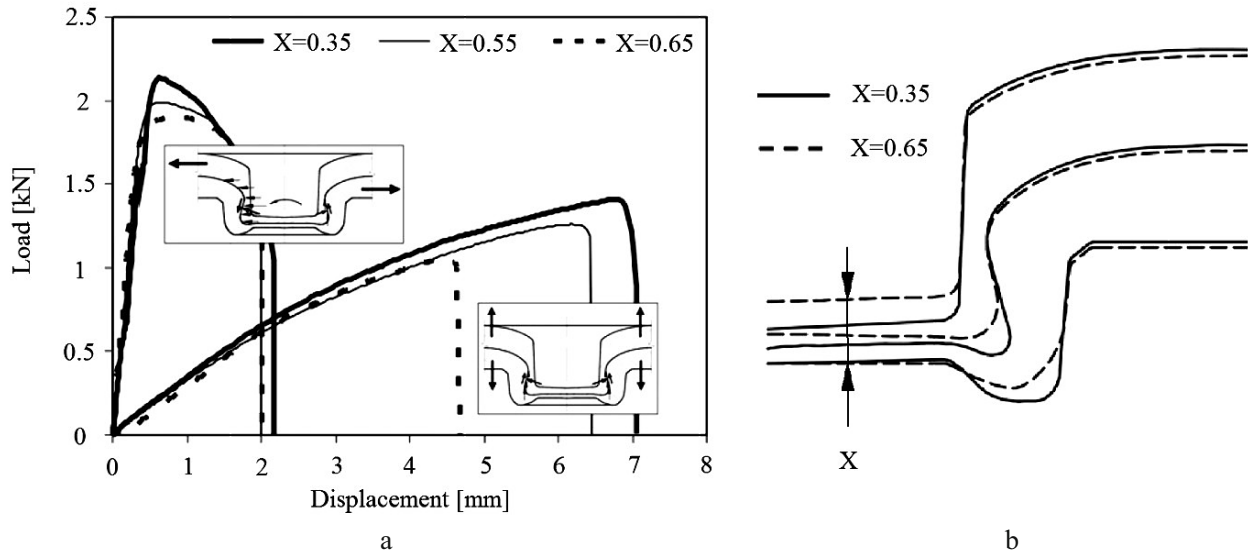Fig. 2. The effect of die depth on joint's undercut and neck thickness [7].



Fig. 3. Load–displacement curves for tensile and tensile–shear tested CL joints (a) and geometries with different bottom thicknesses (b) [8].

joint. The level of interlocking between the upper and lower sheet is the controlling parameter when joint is subjected to tensile load. However, mechanical joints with very low bottom thickness tend to have higher tensile strength than those with higher bottom thickness (Fig. 3) [8].

Mechanically clinched joints can be subjected to experimental or numerical loading conditions. Thus, both approaches are used during the FEA simulation of clinching, in order to compare the resulting geometries or loading forces. Another approach is to evaluate and compare mechanically clinched joints with various parameters, shapes, material combinations or additional layers. The response of a clinched joint (combination of steel and copper sheet) to shear loading is shown in Fig. 4, which depicts different responses of a clinched joint depending on the value of the friction coefficient. It can be seen that the individual clinched joints exhibit different joint failure mechanisms when the coefficient of friction between both sheets varies [9].

Difficult joinability of progressive materials such as advanced high strength steels, or aluminum alloys can be simulated by the FEA. These materials have lower ductility and formability, which often results in cracking or tearing of the upper sheet during the clinched joint forming process. The utilization of finite element modeling makes it possible to change the geometry of tools, process conditions, or to add a cohesive zone model, in order to simulate the failure process of the sheet during the joint forming process. Subsequent changes can be made to specific parts of the total clinching joining process to expand the possibilities of limited joinability of the materials with advanced strength properties, or in general, difficult joinability in terms of mechanical clinching. Moreover, the cohesive zone models (CZMs) are implemented into the finite element models to simulate the gradual decohesion and subsequent failure process of the adhesive layers in the case of hybrid joints [10]. Adhesive layers can be inserted between the
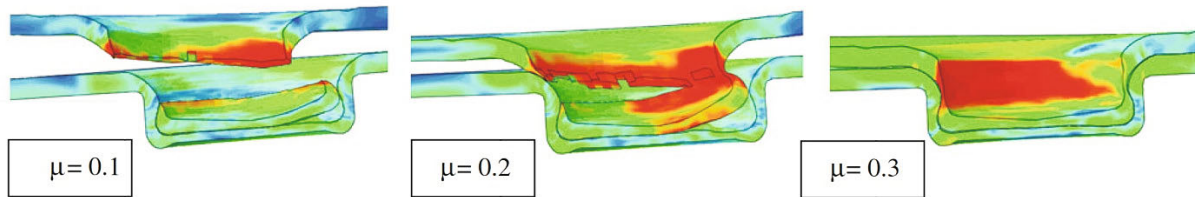
Fig. 4. Responses of the clinched joints to shear load when various values of friction coefficient between the sheets are simulated [9].
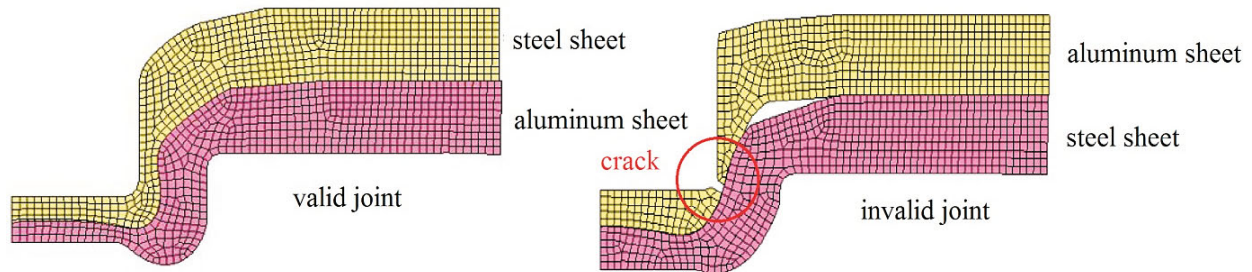


Fig. 5. The application of CZM model when evaluating the joinability of aluminum sheets by clinching [11].

upper and lower sheet when mechanically clinched joint with increased performance is required. Figure 5 shows the application of CZM when joining aluminum and steel sheets in terms of FEA. The valid joint has been produced when aluminum sheet was arranged on the die side (or lower sheet) and steel sheet on the punch side (or upper sheet). The situation changes when positions of sheets are switched. The aluminum sheet on the punch side cracks during the joint forming process. The position of crack is localized in the area that is referred to as the critical zone of a clinched joint. The material in this zone is excessively thinned, which results in cracking, tearing or fracture of the upper sheet before the completion of a clinched joint process formation.

Despite a large scope of scientific work related to mechanical clinching and evaluation of various material combinations, thicknesses, joint shapes, etc., there is a lack of information related to the joining of three sheets' arrangement by mechanical clinching. Finite element model for three steel sheets' joining is described, and the results obtained are discussed in the subsequent sections. In total, three cases are simulated, namely: joining of three DC06, DX53D, and H220PD sheets. Noteworthy is that these cases do not cover any combinations of the above materials.

**2. Simulation Procedure.** This section describes the finite element simulation procedure of the mechanical clinching joining process in terms of the geometrical model, finite element mesh, material model, boundary conditions, contact interactions, and solver settings. The simulation of the joining process was carried out using the commercial ANSYS Mechanical 17 software package in 2D axisymmetric terms. The initial setup of the tools and joined materials that compose the geometrical model is shown in Fig. 6, which also describes the boundary conditions for the individual parts. Noteworthy is that the thickness $t$ parameter of the individual sheets varies as is shown in Fig. 6. Both DC06 and H220PD steel sheets have a thickness of 0.8 mm, while DX53D steel sheet has a thickness of 1.0 mm. Stroke of a punch (parameter $X$ in Fig. 6) also differs. Stroke of 3.4 mm was used for DC06 sheets, 3.42 mm for DX53D sheets, and 3.3 for H220PD steel sheets.

The geometrical model that constitutes the input model for the simulation consists of three rigid bodies (punch, die and sheet holder) and three deformable bodies (steel sheets). Since the tools for mechanical clinching are not in the focus of this study, the computational time can be saved by defining them as rigid bodies. Moreover, tools usually undergo small elastic deformations during their application, hence they are usually modeled as rigid bodies. However, in certain situations (described in Section 1), tools can be defined as deformable bodies. According to the scheme depicted in Fig. 6, the die for mechanical clinching is stationary, while the sheet holder clamps all three sheets by the force of 400 N, and the joint forming process is controlled by the downward motion of a punch (stroke of 3.4 mm).

TABLE 1. Mechanical Properties of Joined Materials

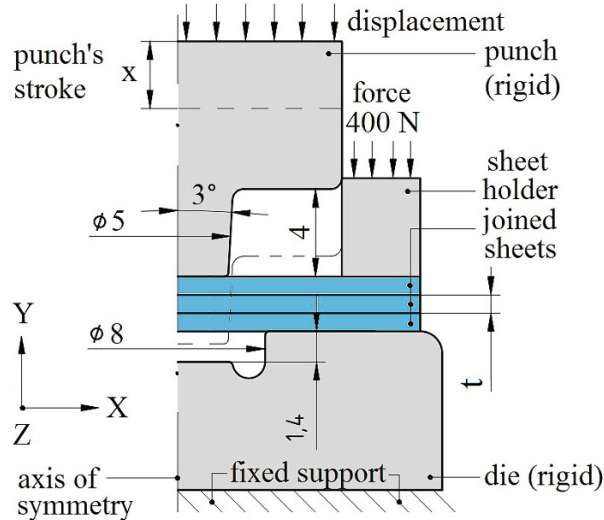| Material | $R_{p0.2}$, MPa | $E$, GPa | $\nu$ |
|----------|-----------------|----------|-------|
| DC06 | 142 | | |
| DX53D | 180 | 210 | 0.287 |
| H220PD | 219 | | |



Fig. 6. The geometrical model and boundary conditions.

       The material model constituting the mathematical representation of behavior of sheets during their deformation consists of elastic and plastic portions, wherein only the elastic modulus and Poisson's ratio are required to define the elastic portion of the material model. The input data for joined materials in this study are listed in Table 1. The plastic portion of the material model was defined by utilizing the multilinear isotropic hardening model. The sheet anisotropy cannot be taken into account by the 2D calculation. Tensile–shear testing of specimens prepared according to the respective standards was adopted to acquire the stress-strain data for DC06, DX53D, and H220PD materials. The stress-strain data were converted from engineering values to the true stress-strain ones, in order to incorporate the input data into the multilinear isotropic hardening material model.

       Deformable bodies in the form of sheets were meshed via the quad-dominant meshing procedure. Lower-order elements had to be used, insofar as the remeshing algorithm is not applicable to higher-order ones. In the ANSYS terms, the 2D axisymmetric elements of PLANE182 type having two degrees of freedom (translational in $X$ and $Y$ directions) were applied to each node. The plasticity, stress stiffening, large deflection, and large strain capabilities are incorporared in this type of elements [12]. To validate the results in relation to the size of elements, a mesh sensitivity study was carried out. The mesh sensitivity analysis has shown that steel sheets having the thickness of 0.8 mm can be meshed by 0.2 mm elements. However, for the better convergence behavior, the elements with the size of 0.1 mm were used. Moreover, sheets with a thickness of 1.0 mm can be meshed via 0.2 mm elements. Another problem related to the FEA of mechanical clinching and the finite element mesh is the mesh distortion during the joint forming process. In order to bypass the excessive distortion of individual elements in the mesh, a nonlinear adaptive region was defined for all three sheets. The following mesh quality criterion was used: if the maximum corner angle of $160°$ in a specific element is exceeded, the remeshing is required. Such elements are either remeshed by the general remeshing scheme, or finer elements are created if the size ratio is set below 1. Figure 7 shows a comparison of the resulting joint (two sheets) with and without repairing the distorted quad-type mesh during the analysis.

       This simulation study was performed for the static implicit conditions. All contacts occurring during the joining process were modeled by frictional interactions with varying friction coefficients. The coefficient of friction
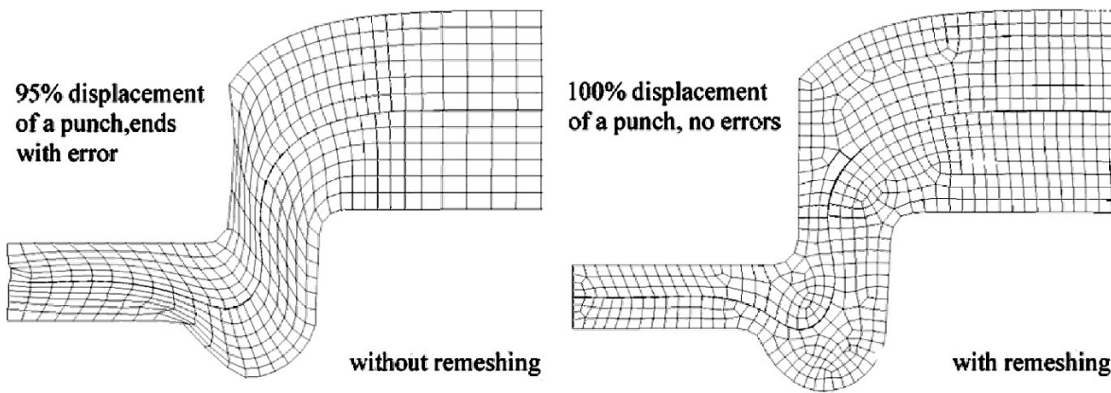
Fig. 7. A comparison between clinched joints with and without remeshing, developed according to [13].
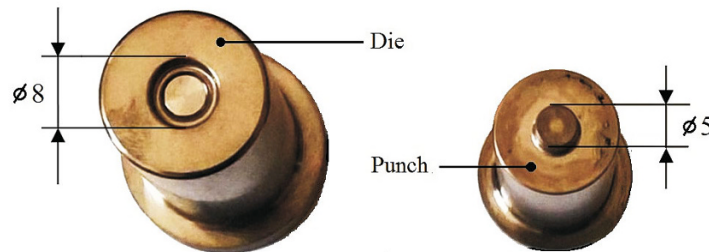


Fig. 8. Experimental die and punch for the mechanical clinching of three sheets.

between the tools and sheets was set to 0.12 and 0.2 for the individual sheets. The incorporation of frictional contacts into the analysis increased the computational time. Besides friction, other nonlinearities such as large-scale contact deformations were present. Given this, the analysis became highly nonlinear, and the asymmetric Newton–Raphson approach had to be utilized. To ensure the convergence behavior of the analysis, the iterative solver was used, which splitted the joint forming process into small iterations (substeps). A less number of substeps can speed up the calculation, but deteriorate the analysis convergence behavior, and vice versa.

**3. Experimental Procedure.** For the direct comparison of the experimental and simulation results, mechanically clinched joints were prepared using a hydraulic press. The experimental tools for mechanical clinching are shown in Fig. 8 and are composed of punch and rigid die with a specially formed cavity. The specimens were prepared according to the STN 05 1122 standard on the shear loading of steel sheets (DC06, DX53D, and H220PD) in the rolling direction. After that, mechanically clinched joints were prepared, tensile– shear tested, and sectioned for metallographic observations. Specimen sections were observed by a Keyence VHX 500 digital microscope. The latter made it possible to measure the specific parameters of mechanically clinched joints, such as the bottom thickness, or neck thickness.

The punch and die for the mechanical clinching (Fig. 8) are made of tool steel for cold work (K390 type, produced by powder metallurgy). Tools have been quenched up to 55 HRC, which resulted in the yield strength of approx. 2000 MPa. This impiled an excellent compressive strength, toughness, and wear resistance. The surfaces of both tools were coated with TiCN coating with a thickness of 2.51 μm deposited by the PVD process. TiCN coatings offer higher hardness, as compared to TiN ones, and can reduce the friction coefficient during sliding of counter-surfaces. Moreover, such coatings improve the resistance to adhesive wear, since zinc from galvanized sheets tends to adhere to the surface of tools.

The mechanical properties of individual joined materials (DC06, DX53D, and H220PD) are shown in Table 2. The parameters listed in Table 2 were acquired via the tensile testing of standard specimens. DC06 is deep-drawing steel utilized for pressed parts with a complex geometry. It can be classified as a low-carbon steel, because the amount of carbon does not exceed 0.02%. DX53D is classified as a hot-dip coated steel, with low carbon content (max. 0.12%) and utilized for cold forming or deep-drawing applications. H220PD belongs in to the

TABLE 2. Thicknesses and Basic Mechanical Properties of Joined Materials

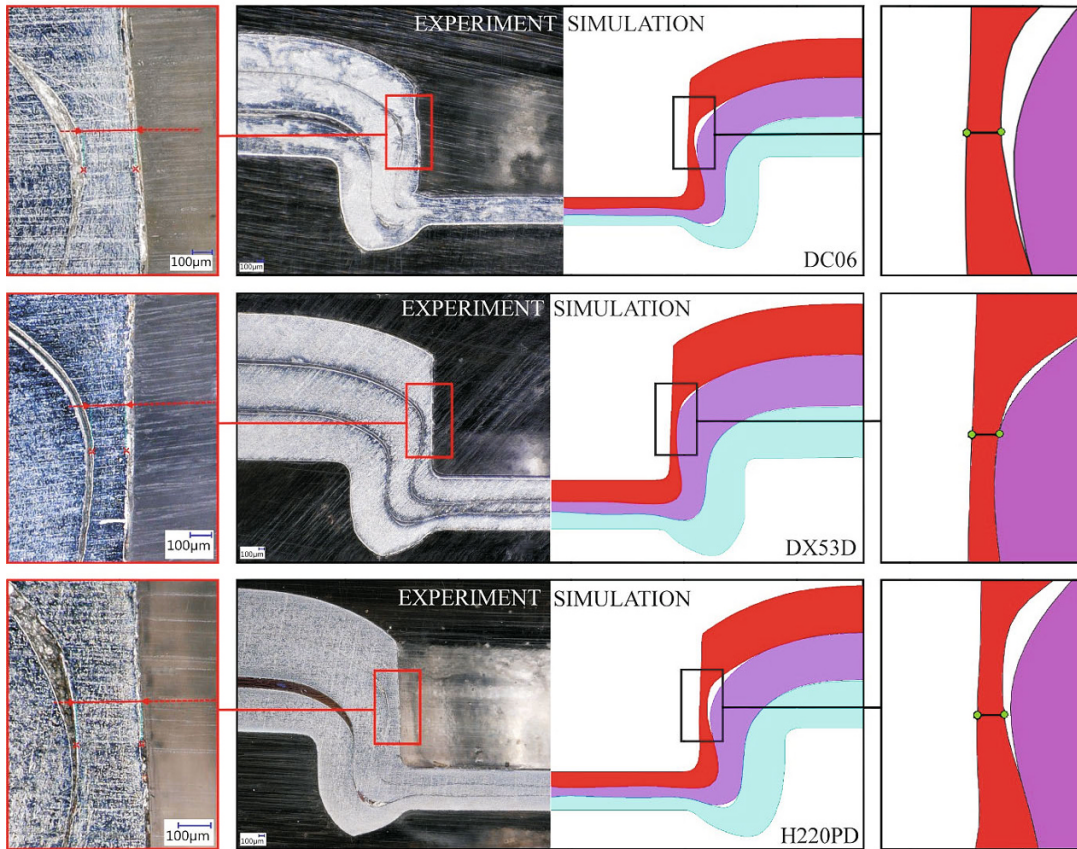| Material | Thickness [mm] | $R_{p0.2}$, MPa | $n$ | $A_{80}$, % | $R_m$, MPa |
|---|---|---|---|---|---|
| DC06 | 0.8 | 142 | 0.214 | 46 | 290 |
| DX53D | 1.0 | 180 | 0.210 | 30 | 270 |
| H220PD | 0.8 | 219 | 0.235 | 34 | 385 |



Fig. 9. Comparison of shapes and neck thickness measuring points for the individual mechanically clinched joints.

non-alloy steel category, which is applicable to the cold forming cases, which require high levels of the yield strength. The maximal carbon content in this steel type is about 0.07%.

**4. Results and Discussion.** This section is mainly focused on the interpretation of results obtained via the finite element simulation of three steel sheets' joining by the mechanical clinching method described in the previous sections. Some experimental results are also shown, because verification of FEA results includes a comparison of results between experimental and simulated approaches. Some FEA results have been processed and acquired by the ANSYS Mechanical APDL environment, which makes it possible to expand the 2D results into the 3D representation when necessary. Moreover, APDL offers more control in terms of plot controls rather than mechanical ones. The deformed geometry, which was obtained by FEA, was exported into CAD environment, in order to assesss the neck thickness of a simulated joint. Figure 9 shows the comparison of geometries of the experimental and simulated joints, which were measured by the digital microscopy (experimental) or assessed by the CAD measuring tools (simulated joint). Steel sheets in the simulated results were filled with color for a better representation of details of individual sheets in the mechanically clinched joints. Figures showing the measurement of neck thickness, in the case of simulated joints, are for representation purpose only. Hence no scale factor is shown in those figures. The resulting neck thicknesses are summarized in Table 3.

TABLE 3. Values of Neck Thickness for Mechanically Clinched Joints

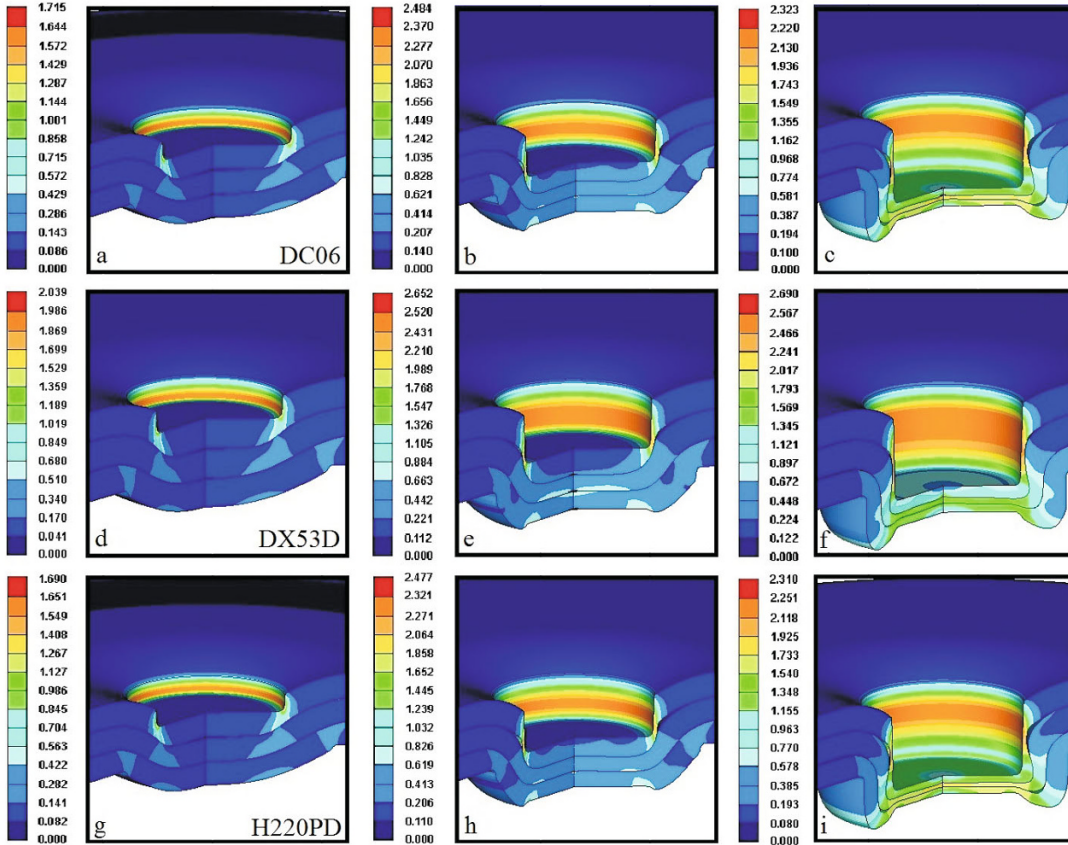| Material | Neck thickness (experiment) [µm] | Neck thickness (simulation) [µm] |
|---|---|---|
| DC06 | 235 | 160 |
| DX53D | 160 | 142 |
| H220PD | 201 | 150 |



Fig. 10. The evolution of plastic strain in steel sheets during individual joint forming phases.

The geometries of the individual joints shown in Fig. 9 are in good agreement with the experimental ones. The individual sheet bottom thicknesses of the simulated joints match the experimental ones. There is a slight difference in the case of DX53D, where the thickness of the bottom sheet of a simulated joint is larger than its counter-joint. Another area that differs from the experimental joint is the height of the protrusion of the upper sheet (marked with a black circle, DX53D joint). Moreover, some gaps between the lower and middle sheet (in the case of DC06 and H220PD) failed to be formed in the simulated results. This could be related to the plasticity model chosen for the simulation, which was not capable of a proper description of the springback effect. Otherwise, these gaps could be formed during the cutting process of the specimens. The large difference in the neck thicknesses was observed in the case of DC06 joint, which was approx. 100 µm. Despite the above differences, the curvature of individual sheets, their thicknesses, and interlocking contours matched the experimental ones quite closely. The plastic strain increments during the individual joint forming phases are shown in Fig. 10, in compliance to those depicted in Fig. 1, with the omission of their start positions. As it was already mentioned, the 2D results were expanded to the 3D representation by the 230° expansion technique.

The plastic strain distributions during the individual joint forming phases (drawing, compression, and interlocking) were very similar for all observed materials. In the initial drawing phase (Fig. 10a, d, and g), the plastic strain occurred in the areas where sheets came into contact with tools or each other. The plastic strain is subsequently
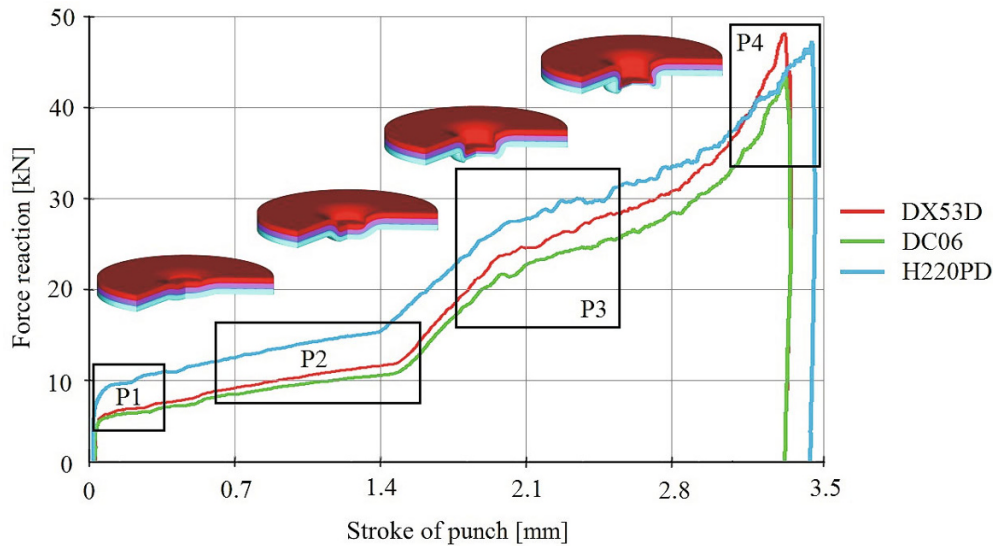
Fig. 11. Development of force reaction in punch in relation to its stroke.

distributed across the thickness of steel sheets with a progressing stroke of the punch. The largest values of plastic strain increment were concentrated in the upper sheet for all three materials. This portion of the sheet is referred to as the critical (neck) area of the mechanically clinched joint. The upper sheet (sheet in contact with punch) is excessively strained and thinned during the total joint forming process. Due to that, the upper sheet often tends to tear when the joint is loaded or even during the joint forming process. However, one cannot take for granted that the upper sheet would tear in the critical neck area, unless a cohesive zone model (CZM) or a damage model are introduced in this simulation, which would simulate the cracking or separation of the upper sheet's neck area. This additional feature would improve the simulation accuracy and make it possible to evaluate the joinability of materials that have insufficient ductility for joining by the mechanical clinching. The following results show the development of force reaction in the punch during its stroke (Fig. 11).

The reaction forces calculated by the FEA of mechanical clinching were compared to the forming forces needed to form the experimental mechanically clinched joints. The latter values were as follows: 40, 45, and 42 kN for DC06, DX53D, and H220PD, respectively. The calculated levels of reaction force (in the global $Z$ direction) in the punch obtained during the simulation of mechanical clinching were as follows: 42, 48, and 46 kN for DC06, DX53D, and H220PD, respectively. It is noteworthy that the reaction forces matched the experimental ones when a certain level of tolerance was taken into consideration. Moreover, the shape of force reaction curve is very similar to that acquired in case of joining two steel sheets. The force reaction development in relation to the punch stroke when joining of two steel sheets can be found elsewhere [14]. The characteristic joint forming phases are marked in Fig. 11 according to the above reference. The deformed geometry related to the individual joint forming phase (along with the level of force and punch stroke) was added to Fig. 11. The geometry of steel sheets should correspond to the level of force and punch stroke, because these are related to the evolution and distribution of the plastic strain in sheets. Regions *P1*, *P2*, *P3*, and *P4* are subsequently defined as the drawing, compression, upsetting, and clinching zones.

Another result of FEA that contributes to the clarification of the joint forming mechanism is the material flow of individual sheets. The material flow for individual steel sheets (DC06, DX53D, and H220PD) during the mechanical joining by means of clinching is shown in Fig. 12. The material flow identified by the finite element analysis makes it possible to comprehend the behavior of individual sheets, as well as the interlock forming phenomena during the joint forming process. Such results display the instantaneous speed of displacement of the material during its plastic deformation. All types of steels used in the experiment tend to behave in a similar manner when they are plastically deformed by the punch and die. At the drawing phase (Fig. 12a, d, and g), the largest material flow (approx. 20 mm/s) is exhibited by the upper sheet, which is drawn into the die cavity by the action of the punch. The instantaneous speed of material slowly decreases towards the lower sheet. There is a change in the
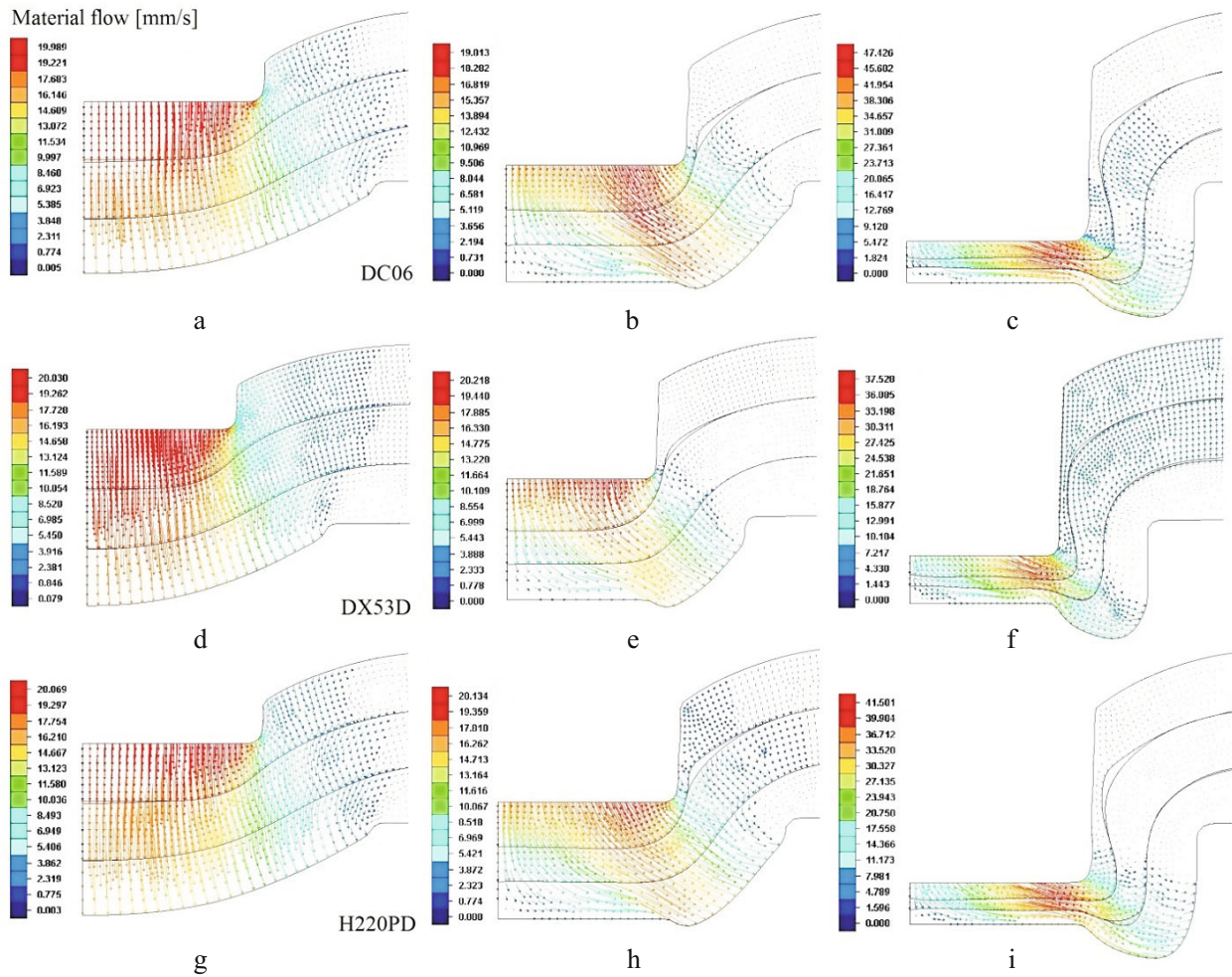
Fig. 12. The material flow in steel sheets during the individual joint forming phases.

material flow when the lower sheet comes into contact with the anvil of the die cavity. This period is also referred to as the compression phase of the mechanical clinching. Since the material has no room to flow downwards, it is forced to flow in the lateral direction towards the groove of the die cavity. This phenomenon is shown in Fig. 12b, e, and h. The speed of material flow, in the case of all simulated materials, does not change drastically. Although the behavior of all steel sheets was similar so far, there was a slight change in the material flow at the final interlocking phase of joining. The lower steel sheets (H220PD and DC06) fill the groove of the die cavity at the interlocking phase (Fig. 12i). The mechanically clinched joint should be fully produced at this point. However, there is a different situation in the case of DX53D steel sheets. The differing thickness (1.0 mm) and stroke of the punch (3.42 mm) caused a slight change in the material flow, as compared to the rest of the materials. This phenomenon, being called "the backward extrusion of upper sheets," occurs when the die cavity is completely filled [15]. This state causes the backward material flow of the upper and middle sheets in the opposite direction to the die cavity. This phenomenon is depicted in Fig. 12f. The instantaneous speed of displacement of material, in the case of all three materials during the interlocking phase, increased almost twice, as compared to those at the previous phases.

The backward extrusion of the upper steel sheet during the mechanical clinching can be taken into account by modifying the geometry of tools, when the particular process conditions should be maintained. The punch protrusion should be tapered to the conic shape, which would physically prevent the upper sheet from extruding backwards during the interlocking phase. It could be also controlled by the die groove shape. The flatter the die groove, the more possibility for backward extrusion of the upper sheet. Finally, one of the additional factors controlling this phenomenon is the sheet stiffness.
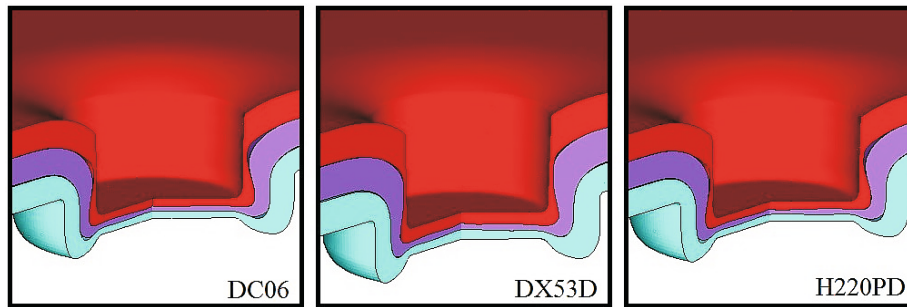
Fig. 13. Final geometries of mechanically clinched joints from DC06, DX53D, and H220PD steels.

The final joint geometries for all materials (DC06, DX53D, and H220PD) obtained by the finite element analysis of a mechanical clinching of three sheets are shown in Fig. 13, where the 2D results for individual clinched joints have been expanded into the 3D axisymmetric representation (230° rotation).

**Conclusions.** The mechanical clinching of three steel sheets (DC06, DX53D and H220PD) was simulated in this study by the finite element method. The joining process was reduced to 2D axisymmetric conditions, and the isotropic material model of joined sheets was applied. The results of FEA were compared to the experimental ones. The comparative analysis of geometries showed that specific areas of mechanically clinched joints (such as the individual sheet thicknesses in bottom and neck area, shape of interlocking area, filling of the die groove by the bottom sheet) calculated by FEA and experimentally obtained are in very good agreement. Only minor differences were found in the case of the mechanically clinched joint of DX53D steel. The largest difference in the neck thickness was observed in the case of DC06 steel. The evolution and distribution of plastic strains in the deformed sheets were similar for all observed materials. The plastic strain was found to initiate in the contact zones between sheets and tools or between the adjoining sheets and then to progress towards the thickness of individual sheets. The peak values of plastic strain were attained in the critical (neck) zone of mechanically clinched joints. This critical zone corresponded to the location with the largest thinning of the upper sheet. The development of reaction forces in the punch during the joining process coincided with the curve shape observed during joining of two sheets. The characteristic joint forming phases could be identified by the shape variation of the individual force reaction curves. The calculated and experimental values of force reactions differed only slightly. One more parameter investigated in this study was the material flow during drawing, compression and interlocking phases of joining. The so-called backward extrusion phenomenon was observed in the case of DX53D steel sheets, which could be attributed to the increased thickness of joined sheets, in contrast to the other materials under study. At the interlocking phase of joining, thicker sheets filled the volume of the die cavity before reaching the preset punch stroke. At this point, the middle and upper sheets tended to flow out of the die cavity. This deficiency can be bypassed by the tool geometry modification. The results of finite element modeling of clinching joining of three sheets can be utilized in the future works. Since the upper sheet undergoes large plastic deformation and excessive thinning during the joining process, the upper sheet model should be replaced with a more advanced one capable of simulating the material separation or cracking. This could improve the simulation accuracy, making it possible to evaluate the joinability of materials. Moreover, the resulting joints can be loaded by different types of loading, in order to evaluate their load-bearing capacities. The obtained results on three sheets' clinching joining can be also used for two-sheets' mechanical clinching applications.

**REFERENCES**

1.     F. Lambiase and A. Di Ilio, "Damage analysis in mechanical clinching: Experimental and numerical study," *J. Mater. Process. Tech.*, **230**, 203–210 (2016).

2. C. Chen, S. Zhao, M. Cui, et al., "An experimental study on the compressing forces for joining Al6061 sheets," *Thin Wall. Struct.*, **108**, 56–63 (2016).

3. T. Jiang, Z.-X. Liu, and P.-Ch. Wang, "Effect of aluminum pre-straining on strength of clinched galvanized SAE1004 steel-to-AA6111-T4 aluminum," *J. Mater. Process. Tech.*, **215**, 193–204 (2015).

4. F. Lambiase, A. Paoletti, and A. Di Ilio, "Advances in mechanical clinching: employment of a rotating tool," in: Proc. of the 17th Int. Conf. on Sheet Metal (SHEMET17), Vol. 183 (2017), pp. 200–205.

5. K. Mori, N. Bay, L. Fratini, et al., "Joining by plastic deformation," *CIRP Annals*, **62**, No. 2, 673–694 (2013).

6. A. A. de Paula, M. T. P. Aguilar, A. E. M. Pertence, and P. R. Cetlin, "Finite element simulations of the clinch joining of metallic sheets," *J. Mater. Process. Tech.*, **182**, 352–357 (2007).

7. Y. Zhou, F. Lan, and J. Chen, "Influence of tooling geometric parameters on clinching joint properties for steel-aluminum hybrid car-body structures," in: Proc. of the Computer Science and Information Technology (ICCSIT), Vol. 5 (2010), pp. 441–445.

8. J. Mucha, "The analysis of lock forming mechanism in the clinching joint," *Mater. Design*, **32**, No. 10, 4943–4954 (2011).

9. T. Sadowski, T. Balawender, and P. Golewski, *Technological Aspects of Manufacturing and Numerical Modeling of Clinch-Adhesive Joints*, Springer, New York (2015).

10. T. Sadowski, P. Golewski, and E. Zarzeka-Raczkowska, "Damage and failure processes of hybrid joints: Adhesive bonded aluminum plates reinforced by rivets," *Comp. Mater. Sci.*, **50**, No. 4, 1256–1262 (2011).

11. P. Kamble and R. Mahale, "Simulation and parametric study of clinched joint," *Int. Res. J. Eng. Technol.*, **3**, 2730–2734 (2016).

12. *ANSYS 17.0 Documentation, ANSYS Mechanical APDL Element Reference*, ANSYS Inc., Canonsburg, PA (2013).

13. V. Hamel, J. M. Roelandt, J. N. Gacel, and F. Schmit, "Finite element modeling of clinch forming with automatic remeshing," *Comput. Struct.*, **77**, No. 2, 185–200 (2000).

14. P. Siedlaczek, "Numerical analysis and test simulation of clinch forming," in: *Research and Development Directions of Cold Clinch Joints* [in Polish], Oficyna Wydawnicza Politechniki Rzeszowskie, Rzeszów (2015).

15. C. J. Lee, J. M. Lee, H. Y. Ryu, et al., "Design of hole-clinching process for joining of dissimilar materials-A16061-T4 alloy with DP780 steel, hot-pressed 22MnB5 steel, and carbon fiber-reinforced plastic," *J. Mater. Process. Tech.*, **214**, No. 10, 2169– 2178 (2014).